Computational Fluid Dynamics (CFD) Modeling of Novel Designs For 3D-Printed Spacers in High-Pressure Membrane Modules

*Zuo Zhou, David A. Ladner**

Department of Environmental Engineering and Earth Sciences, Clemson University
Clemson, South Carolina 29625, United States

**Corresponding author, David A. Ladner: 864-656-5572, ladner@clemson.edu*

Key words:

CFD, desalination, thin-film composite membranes, 3D-printed spacers

Abstract

In the recent decade, 3D printing technology has been used to produce spacers in the membrane industry due to its advantages at dealing with complicated geometries and simplifying the assembling process. A new spacer methodology is investigated that uses 3D printing to directly attach spacers to the membrane surface. The novelty of this method is that the spacer channels can be built thinner, which leads to smaller spacer heights. Therefore, within the same module volume, more layers can be packed and more surface area can be created to achieve higher permeate flux. The research goal is to design efficient models that help us discover the best parameters for 3D-printed spacers. Spacer heights and spacer patterns are directly related to pressure drop and concentration polarization (CP). Thus, computational fluid dynamics is useful in helping expedite the process of discovering the best designs with both low pressure drop and low CP. Simulations investigated spacer shapes including regular cylinders, elliptical cylinders, and airfoils. Spacer heights ranging from 200 μm to 500 μm were simulated to discover the height to achieve the same pressure drop as a 30 mil conventional spacer. Simulation results indicate that 3D-printed spacers with elliptical design can greatly increase water productivity in a spiral-wound module by increasing packing capacity. These designs also reduce CP by improving the hydrodynamics. Ellipses with a length:width ratio of 2.4 were optimal.

1. Introduction

Reverse osmosis (RO) membranes are extensively used as a desalination technology [1], and are experiencing rapid growth in both municipal and industrial water treatment [2,3]. One problem that exists in all RO systems is the high capital and operating cost to build and maintain an RO system. To reduce capital cost, it is important to improve the performance of the membranes. Among all the methods to achieve high performance of the membranes, one of them is to enhance permeate flux through spacers, which alter the flow and mass transfer patterns, and therefore affect the permeate flux [4]. In addition, membrane area could be increased through reducing the thickness of spacers, which improves the packing capacity of the membrane module. By promoting mass transfer and improving water productivity, spacers can help improve the hydrodynamics of the RO system [5–8]. Therefore, the capital cost of the system can be reduced.

Feed spacers are used in spiral wound membrane modules to create intermembrane space and increase water mixing [9]. Due to its important role in the membrane field, many groups have done research numerically and experimentally to improve the design of the spacers [10–13]. Different geometries such as ladder shapes, diamond shapes [14–17], spacers with modified filaments or twisted tapes, and multi-layer spacers [18] were investigated and their mass flow results were studied. However, due to the limitations of conventional manufacturing method, the complexity of these spacers are still limited. Therefore, in recent years, 3D printing technology has gained attention in building and designing spacers [19].

Research groups have focused on different aspects of 3D-printed spacers. Yanar et al. analyzed membrane spacer materials and discovered that certain printing materials can effectively reduce fouling [20]. Lee et al. [21] looked into 3D printing technologies based on solid, liquid, and powder, assuring its potential for membrane module designs. With the help of 3D printing technology, new spacer geometries have emerged, such as sinusoidal spacers [22], wave-like spacers [23], pillar-like spacers [24], column shaped

spacers [25], and triply periodic minimum surface spacers [19]. These spacers validated the accuracy of 3D printing technology, and also showed improved performance through reducing membrane fouling, or improving energy efficiency.

The unique aspect of the spacers that we are discussing in this paper is that it uses 3D printing technology to directly print spacers onto the membrane surface, which is different from the spacers in much of the published work. Spacer materials include food grade polymers, food grade epoxies, thermoplastics, and waxes [26]. 3D printed spacer thickness can potentially be as low as 5 mil (0.13 mm), which is much thinner than conventional spacers that are usually between 26 and 34 mil (0.66 mm and 0.86 mm) [9]. These spacers can greatly increase the amount of membrane area packed in a membrane system, and therefore increase the flow rate of clean water that can be produced within a single module. Compared with conventional spacers, these 3D-printed spacers have much higher packing capacity within the same module volume.

One concern with thinner spacers is that longitudinal pressure drop can increase, which increases energy consumption. Therefore, it is suggested that a thin feed channel spacer with low pressure loss at a high mass transfer rate can be advantageous for improved water productivity [27]. For our 3D-printed spacers, they take up much less cross-sectional area than conventional spacers. Therefore, it is reasonable to believe that the spacers will not cause extra pressure drop under lower spacer height.

Computational fluid dynamics, as a widely used analysis tool in membrane separations [28], is adopted to simulate the fluid flow through numerical methods and equations [29]. In this research, the first step is to compare pressure drop between traditional mesh spacers and novel printed spacers, and then an automated simulation system is built for all the 2D models to select through all the potential geometries. 3D models will be conducted to help discover the best designs in terms of pressure drop and concentration polarization.

2. Materials and methods

A variety of simulations was performed in both 2D and 3D. 3D simulations were first conducted to compare the pressure drop in channels filled with conventional spacers and 3D-printed circular pillar spacers. These 3D simulations help discover the channel height for 3D-printed spacers in order to reach the same pressure drop as a channel filled with conventional spacers. After deciding on the channel height, 2D simulations were run to discover the best spacer designs. More 3D simulations were conducted again to apply the 2D designs in a realistic 3D system to investigate concentration polarization.

2.1 Geometries studied

2.1.1 3D geometries for pressure drop studies

In this simulation, a membrane channel with conventional spacers is first built to investigate its pressure drop. Then several channels filled with 3D-printed spacers were evaluated with heights varying from 100 μm to 500 μm.

Our simulations for conventional spacers are based on the diamond-shaped ones. The channel height is set to be 0.76 mm (30 mil) which is a common thickness for spacers. The conventional spacer height is equal to half of the channel height and they are placed on top of each other. Traditional spacers require larger computing capacity due to their complex geometry. Therefore, the models try to simulate a minimum length while achieving reasonable results. Models with different domain lengths including 6 mm, 12 mm, 18 mm, and 24 mm were simulated and pressure drop values were compared. At 12 mm, pressure drop per length reached to a stable value, so we carefully chose 12 mm as the domain length (Figure 1 a and b). The domain width is 6 mm.

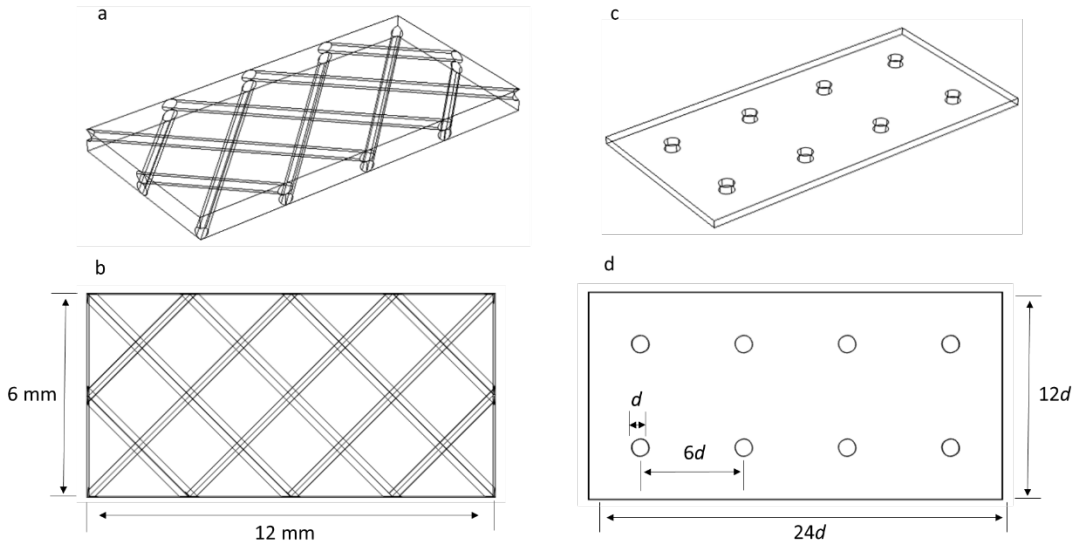

Figure 1. Membrane channels with conventional spacers (a and b) and 3D-printed spacers (c and d). The height of the conventional-spacer filled channel is 0.76 mm, while the height of the 3D-printed spacer filled channel varies in the first series of studies by performing a parametric sweep.

For 3D-printed spacers, four rows and two columns of circular spacers were simulated. More shapes will be investigated later in the paper. Here, the spacer parameters are based on a design that has been prototyped in which the ratio of spacer length and distance between the centers of two nearby spacers is equal to 1:6 [26]. In these models, we study the spacers when *d* is 1 mm and compare the results with the conventional spacers. A conceptual model is built to help explain the boundary conditions (Figure 2). The feed enters the domain on the left side, and the permeate leaves the domain on the right side. The top surface indicated in grey is where the membrane is located, and the rate of permeation is calculated in Equation 1. The inlet velocity changes according to the channel height, making sure the volume flow rate is the same among all simulations.

$$u_m = A(\Delta P - a_{osm} c_w) \quad (1)$$

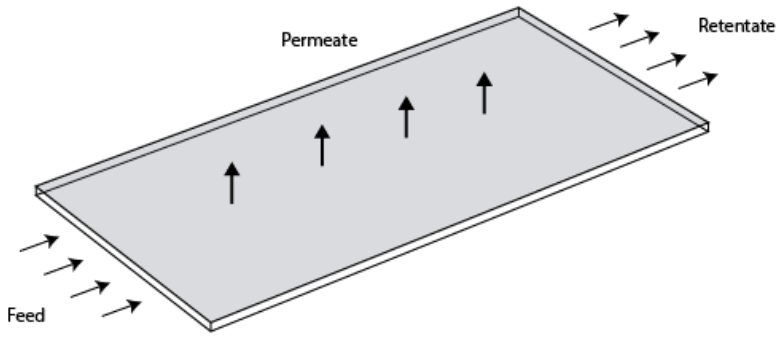

Figure 2. Conceptual model for 3D geometries.

2.1.2 2D geometries

Dozens of RO membrane models assembled with varied spacers were built for analysis. In this study, only one single element was investigated in each model. The geometries include cylinders, elliptical cylinders, and airfoils. These shapes have smooth features that could potentially reduce drag and improve hydrodynamics. They allowed an investigation of the hydrodynamic effects of different surface features. Spacers were set to have the same width, the same length, or the same attached area to the membrane surface to investigate how feature widths and feature lengths can affect the pressure drop results. All models were created with COMSOL Multiphysics 5.5.

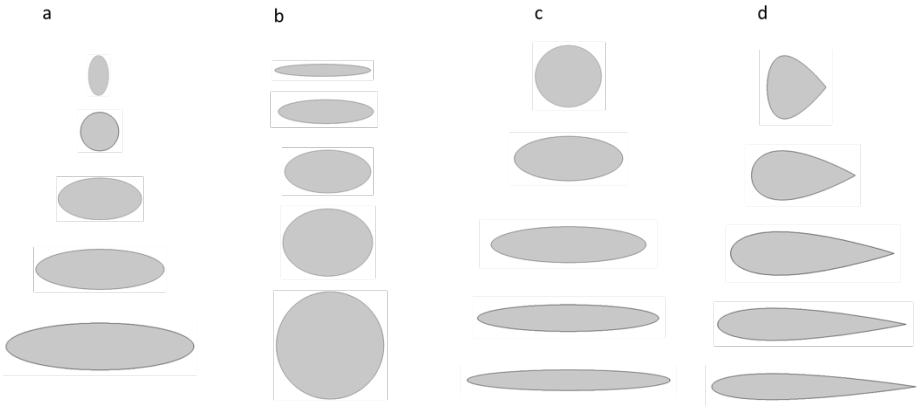

Figure 3. Spacer geometries. (a) Ellipses with the same width (1 mm) but different lengths (0.5 mm to 4 mm). (b) Ellipses with the same length (4 mm) but different widths (0.5 mm to 4 mm). (c)(d) Ellipses and airfoils with the same total area, but different x-axis and y-axis lengths. The x-axis length ranges from 1 mm to 3 mm for 2D simulations, and y-axis length ranges accordingly.

2.1.3 3D geometries for concentration polarization studies

3D geometries were built to investigate concentration polarization (CP) in different models. These geometries were matching the experiments we are planning to conduct in the lab with SEPA cell (Figure 4). The size of the cell is 146 mm in length, 95 mm in width, and 0.42 mm in height.

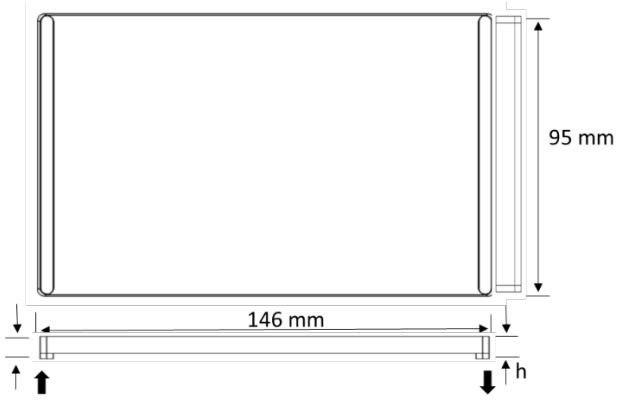

Figure 4. SEPA test cell in the lab.

To determine the ideal parameters of the 3D-printed spacers including the diameter and the distance, a series of calculations was performed shown in Figure 5. In these calculations, our goal is to find the maximum distance between spacers while making sure the membrane channels are still well separated by spacers, given a spiral wound unit with the inner diameter of 19 mm and 29 mm. These two inner diameters are commonly used in the industry. For the circular pillars, the assumption is that the spacer height (h) is equal to the spacer length or diameter (d). Each simulation domain includes four rows of features in two columns, and the distance D is determined through Equations (2)-(5).

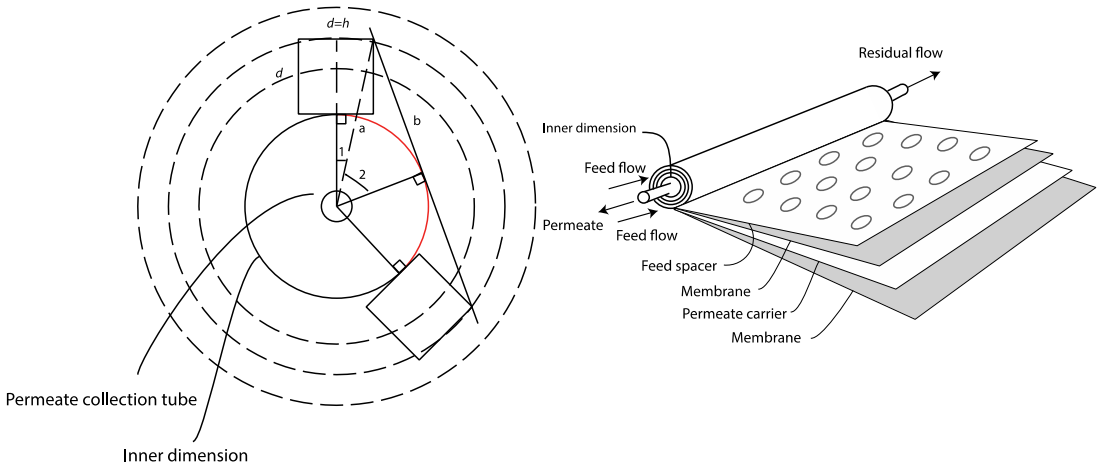

Figure 5. Calculation of spacer distance (indicated in green color in the figure) based on a permeate tube of a spiral wound element with an inner dimension of 19 mm (r = 9.5 mm).

To calculate the arc length in the circle, first calculate a:

$$a = \sqrt{(r+h)^2 + \left(\frac{h}{2}\right)^2} \quad (2)$$

Then calculate b:

$$b = \sqrt{a^2 - r^2} \quad (3)$$

Angle ($\theta + \gamma$) can be derived after calculating the values for tangent a and tangent b:

$$\theta = \arctan\left(\frac{0.5h}{r+h}\right),\ \gamma = \arctan\left(\frac{b}{r}\right) \quad (4)$$

After knowing the angle $\theta + \gamma$ we are able to calculate the arc length, also known as the spacer distance D indicated in red color:

$$D = 2 \cdot 2\pi r \frac{\theta+\gamma}{360°} \quad (5)$$

Under these calculations, for a spacer that has a 0.42 mm in length and 0.42 mm in height, the distance between spacers is 6 mm and 7.3 mm respectively when the inner diameter of the membrane unit is equal to 19 mm and 29 mm.

Different offsets were also studied with the geometries having different staggering levels. Staggering level percentage ranges from 0% when the patterns are perfectly in line and 100% when the patterns are completely staggered (Figure 6).

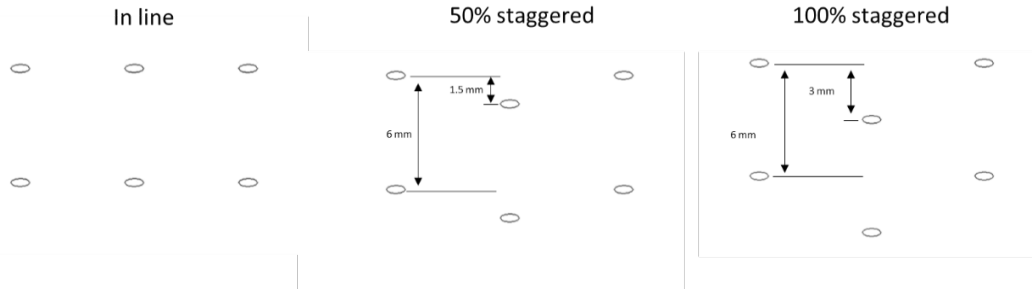

Figure 6. Spacer offsets including in-line and staggered-ones. The 100% staggered offset is when the second row of spacers fall in the middle of the first row.

2.2 Mesh generation

For 2D models, triangular meshes were built and the number of elements were in the same magnitude for all models. A mesh sensitivity test was conducted to make sure that the mesh density change would not have a big influence on the results. For 3D models, tetrahedral meshes were generated and mesh sensitivity test was conducted. More information can be found in the supplemental material.

2.3 Governing equations

The first two parts of simulations include only fluid flow. Therefore, the equations used are Equations (6) and (7). For the last part of simulations, fluid flow and transport of solute were described by Equations (7) - (8)

$$\rho(\nabla \cdot \mathbf{u})\mathbf{u} = -\nabla P + \mu \nabla \cdot (\nabla \mathbf{u} + \nabla \mathbf{u}^{T}) \quad (6)$$

$$\nabla \cdot \mathbf{u} = 0 \quad (7)$$

$$\mathbf{u} \nabla \cdot c = D \nabla^2 c \quad (8)$$

where $\boldsymbol{u}$ is fluid velocity, t is time, ρ is density, P is pressure, μ is dynamic viscosity, and c is concentration. Equation (6) is the Navier-Stokes equation that is used to describe the motion of fluid. Equation (7) is the continuity equation. Equation (8) is the convection-diffusion equation. Momentum and mass transport were fully coupled in the sense that the Navier-Stokes, continuity, and convection-diffusion equations were solved simultaneously, and flux was set as a boundary condition to calculate the concentration profile. Solutions were found using COMSOL Multiphysics 5.5 run on the Palmetto Cluster, Clemson University's primary high-performance computing resource.

3. Results and discussion

3.1 Pressure drop for spacers with different heights and geometries

Pressure drop is first studied in membrane systems with conventional spacers and 3D-printed spacers. Conventional spacer height is set at 30 mil (0.76 mm), while a parametric study for 3D-printed spacers is conducted with varying heights. The study domain is the same as the one in Figure 1. Pressure drop

results are shown in Figure 7 when maintaining the same inlet velocity (a) or volumetric flux (b). As the spacer heights decrease, pressure drop results increase.

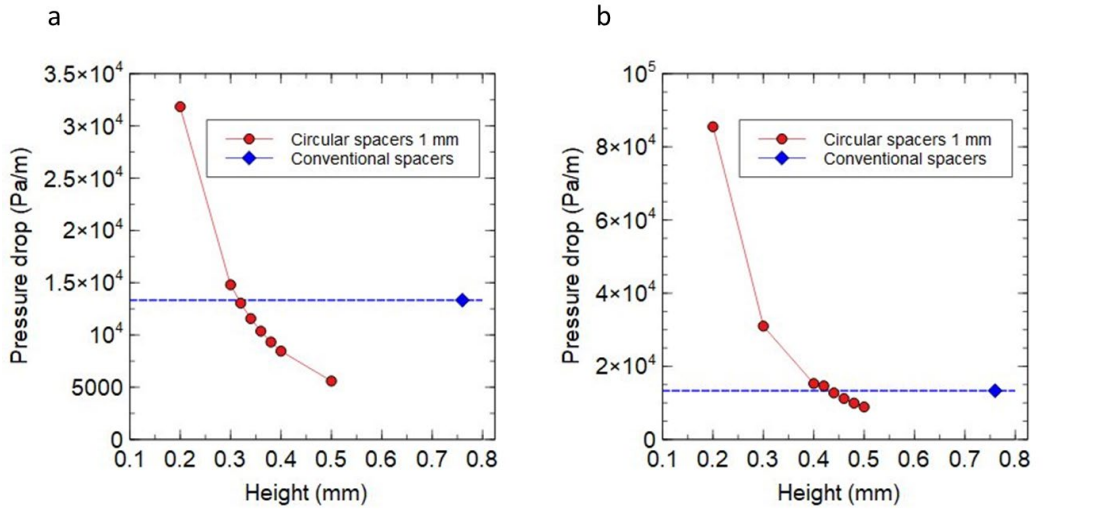

Figure 7. Pressure drop for 3D-printed spacers forming various channel heights under (a) constant crossflow velocity and (b) constant volumetric flow rate.

The blocking area of the two channels are calculated. In our simulations, the conventional spacer blocking percentage is 3.2% and the 3D-printed spacer is 2.2%. Literature review was conducted to estimate the percentage in common spacer filled channels that are in practice. Calculation shows that the percentage can range between 3.9% and 8% (see supplemental material) [30]. Reduced blocking area can be beneficial for improving permeate flux within one layer of permeation.

Results show that given the same velocity, to achieve the same pressure drop, 3D-printed spacers had a height of 0.32 mm (Figure 7a), which is less than half as thick compared with conventional spacers. Therefore, within the same volume, when using 3D-printed spacers instead of conventional spacers, one is able to pack in much more layers. One might wonder since the channel height is thinner, if there would be less water being treated in the channel. Therefore, a comparison with the same volumetric flow rate is also plotted where all channels maintain the same flow rate of water being treated while the height is changing. Decreasing channel height causes the crossflow velocity to increase. The results show that the

thickness of the 3D-printed spacers is 0.42 mm (Figure 7b), still much lower than the conventional one. Based on a typical spiral wound membrane unit in Figure 5, modules are assembled with each membrane "sandwich" containing one layer of spacer, one layer of membrane, one layer of permeate carrier, and another layer of membrane. Assuming the inner and outer dimension is 19 mm and

After deciding the channel height for 3D-printed spacers, single elements in 2D simulations were studied to see how the geometries would affect the pressure drop results. At first, both ellipses and airfoils were studied. The area is maintained as the same while lengths and widths being changed (Figure 8). Results show that ellipses and airfoils perform more or less the same and that airfoils did not show much more improvement than ellipses. Therefore, more simulations were focused on ellipses as it is easier to manufacture them. In Figure 9, ellipses are studied varying only lengths or widths. Cylinders are also studied when the length and width are the same. Results show that ellipses work better than cylinders when given the same length or same width. The best pressure drop result occurs when length to width ratio is 2.4.

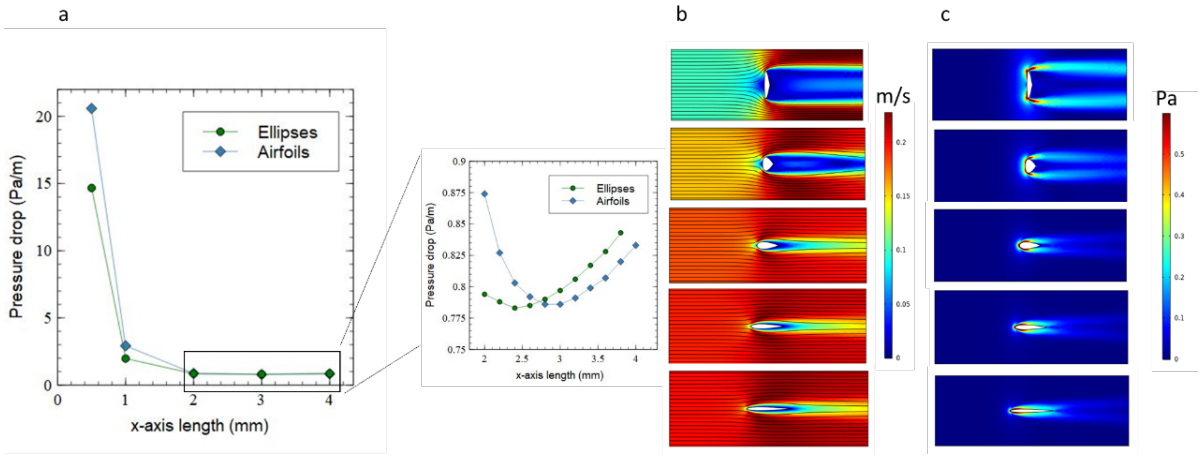

Figure 8. Results for ellipses and airfoils with different x-axis lengths. Figure a is the pressure drop results for both ellipses and airfoils, Figure b shows the velocity profile for airfoils, and Figure c shows the shear stress profile for airfoils.

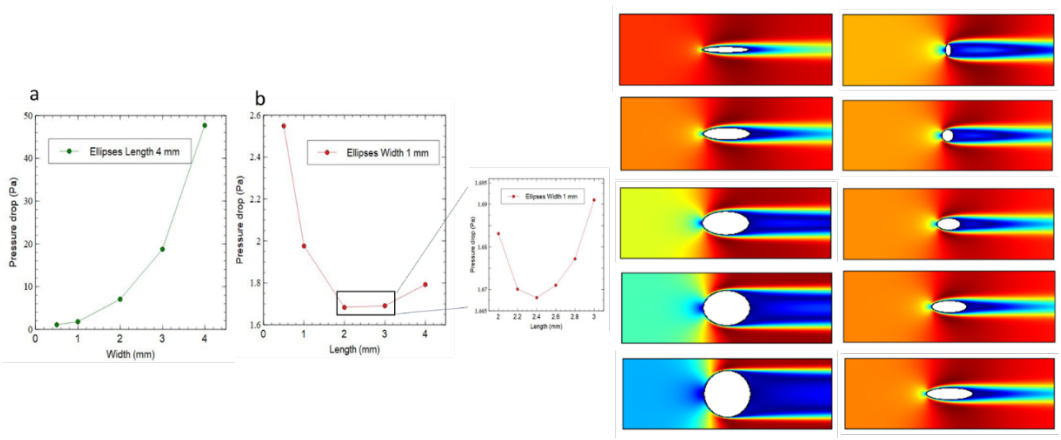

Figure 9. Results for ellipses with varying widths or lengths. In (a), ellipses all had the same length (4mm) but the widths varied from 0.5 mm to 4 mm. In (b), ellipses all had the same width (1 mm) but the lengths varied from 0.5 mm to 4 mm. More simulations for different constant lengths and widths are conducted and are discussed in the supplemental material.

It is quite straightforward to notice that when maintaining the same length while changing widths, pressure drop increases when width increases (Figure 9a). In Figure 9b, pressure drop first decreases dramatically when the x-axis length of the geometries increases while the width stays the same. This is because shear stress has been decreased as the x-axis length increases. When the x:y axis length ratio reaches 2:1 to 3:1, pressure drop value reaches the lowest. Then as the x-axis length keeps increasing, pressure drop starts to increase again because the drag around the shapes increased. A more thorough study about the best length to width ratio is studied. Results show that when the ratio equals 2.4:1, pressure drop is the lowest. This is when setting the ellipse width as a constant number and only changes the lengths. According to Figure 8, when varying both widths and lengths at the same time and keeping the total area the same, the best ratio is 2.6:1 for ellipses and 2.8:1 for airfoils. From these studies the conclusion is that when the spacer width is determined, increasing spacer length will increase pressure drop. However, when the spacer length is determined while the width is changing, the best result for pressure drop is when the length and width ratio is between 2:1 and 3:1. The studies on these single elements give us a direction on designing geometries with low pressure drop, which saves energy and therefore reduces the cost of an entire membrane unit.

3.2 Concentration, shear stress, and permeate flux

For simulations including salt concentration, the models are first validated through comparing 2D and 3D results. The results show similar curves, giving us confidence that the models are behaving well.

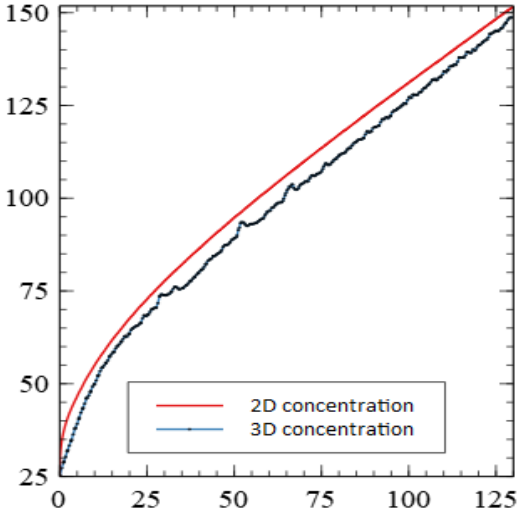

Figure 10. 2D and 3D concentration results for geometry with a length of 130 mm.

Concentration profile was characterized on both an empty channel and channels filled with 3D printed spacers, and the quantitative results are shown through the calculation of CP factor, which is defined as the surface concentration (c_m) to bulk concentration (c_b). 3D printed spacers with elliptical cylinders (length:width = 2.4:1) have in-line and staggered offsets. The comparison for CP, shear stress, and permeate flux profile is shown in Figure 11. Shear stress profile shows the distribution of shear stress at different locations of the membrane channel. It can be observed that adding spacers increased shear stress especially at the places around the spacers. Concentration and shear stress profiles help us see how the hydrodynamics of the channels have changed due to the addition of the spacers. Permeate results show that membranes with patterns successfully improved permeate flux, especially towards the end of the channel. The average permeate flux result is shown in Figure 12, giving us a more quantitative understanding. Permeate results show that membranes with patterns successfully improved permeate flux, especially towards the end of the channel. The average permeate flux result is shown in Figure 12, giving us a more quantitative understanding.

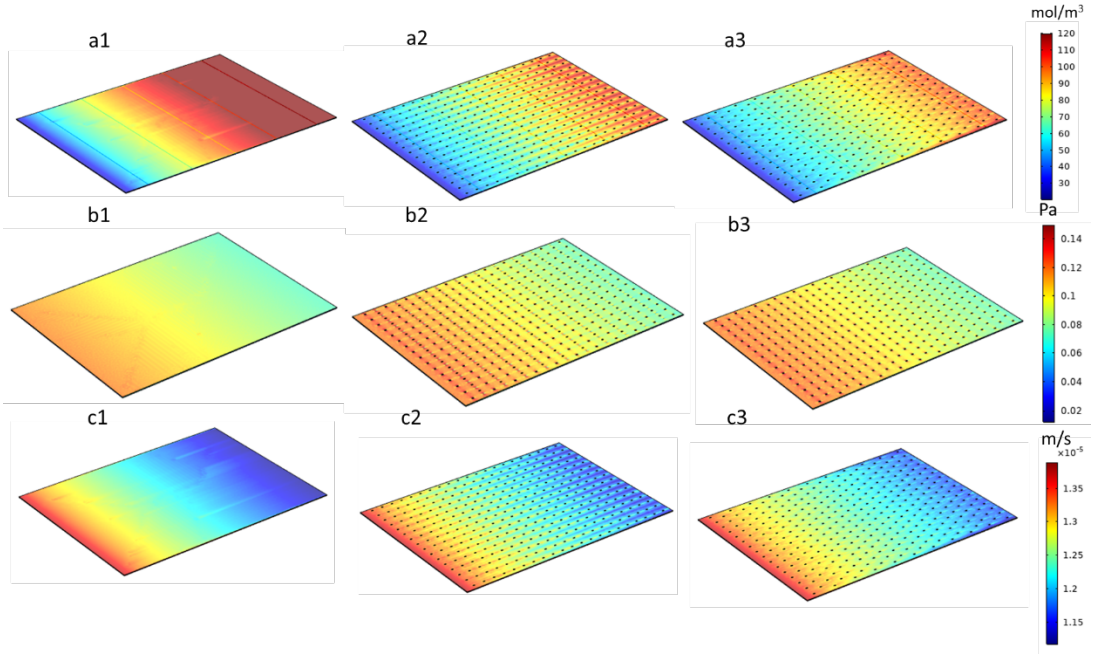

Figure 11. Concentration profile for (a1) an empty channel, (a2) a channel filled with in-line spacers, and (a3) a channel filled with staggered spacers. Shear stress profile for (b1) an empty channel, (b2) a channel filled with in-line spacers, and (b3) a channel filled with staggered spacers. Permeate flux profile for (c1) an empty channel, (c2) a channel filled with in-line spacers, and (c3) staggered spacers. All channel heights are 0.42 mm. All spacers are in an elliptical shape with a length of 1 mm and a width of 0.42 mm. The distance between features is 6 mm.

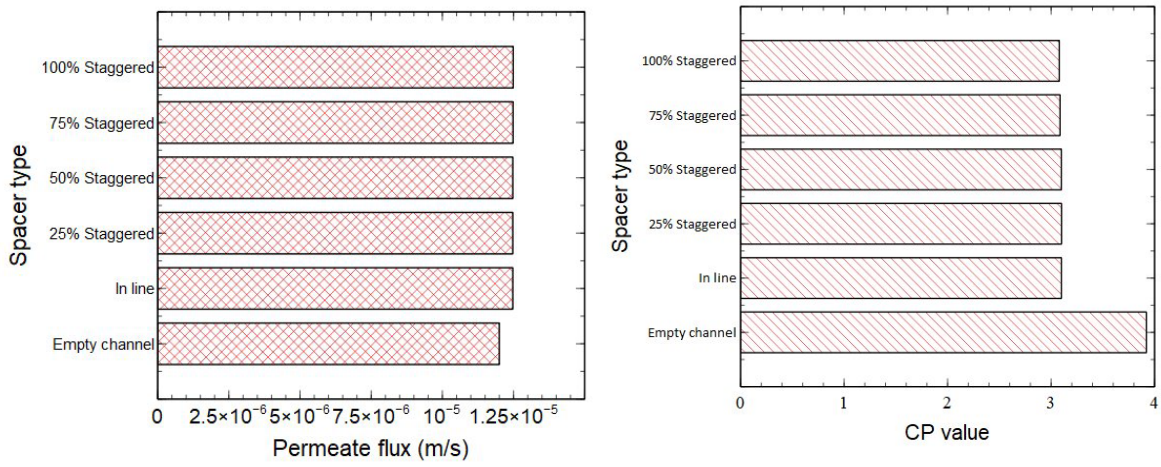

Figure 12. CP and permeate flux results for models with an empty channel and spacers with different staggering levels. The staggering degree goes from 0% (completely in-line) to 100% (completely staggered).

3.3 Velocity profile and streamlines

The system has a low Reynolds number (around 20) due to its thin channel height. Velocity profile fits the planar Poiseuille flow and is under laminar flow pattern. Part of flat membrane's side view of the velocity profile is shown below. Like the concentration results, 2D and 3D models are both simulated and a matching curve is discovered to prove the accuracy of the models.

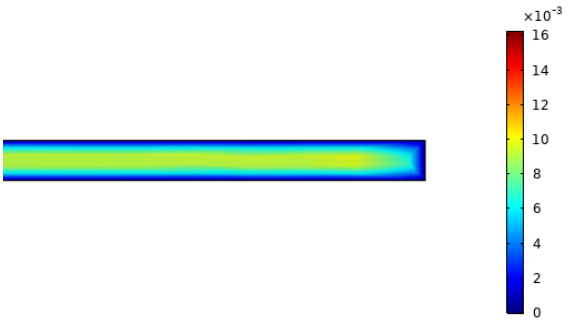

Figure 13. Velocity profile for the side view of the channel. The profile fits a typical laminar flow.

4. Conclusions

3D printed spacers with improved hydrodynamics and packing capacity were evaluated using computational models. Both 2D and 3D models were built to expedite the discovery of the best arrangement. Results show that 3D spacers that are directly printed onto the membrane surface can enable modules to be built with thinner feed channels than conventional designs while having the same pressure drop. Thinner feed channels would mean the packing capacity is greatly increased compared to conventional spacers. Circles, airfoils, and ellipses were all investigated under different lengths and widths, and in the end, one shape was determined with a proper length to width ratio for the best performance. A practical solution was also found through calculating the parameters based on a realistic reverse osmosis membrane unit. Among all the simulations, the best design is elliptical cylinders with a length to width ratio equal to 2.4, and a between-feature distance of 6 mm. The layout of the spacers did

not play a big role in changing the concentration results; however, all channels filled with spacers reduced CP by 21% compared to an empty channel.

Acknowledgements

The authors gratefully acknowledge funding through the Designing Materials to Revolutionize and Engineer our Future (DMREF) program of the U.S. National Science Foundation, grant number 1534304. We also acknowledge computational support through the Palmetto Cluster, Clemson University's primary high-performance computing resource.

References

[1] T. Ishigami, K. Amano, A. Fujii, Y. Ohmukai, E. Kamio, T. Maruyama, H. Matsuyama, Fouling reduction of reverse osmosis membrane by surface modification via layer-by-layer assembly, Sep. Purif. Technol. 99 (2012) 1–7. https://doi.org/10.1016/j.seppur.2012.08.002.

[2] C. Fritzmann, J. Löwenberg, T. Wintgens, T. Melin, State-of-the-art of reverse osmosis desalination, Desalination. 216 (2007) 1–76. https://doi.org/10.1016/j.desal.2006.12.009.

[3] D.E. Potts, R.C. Ahlert, S.S. Wang, A critical review of fouling of reverse osmosis membranes, Desalination. 36 (1981) 235–264. https://doi.org/10.1016/S0011-9164(00)88642-7.

[4] S. Ma, L. Song, Numerical study on permeate flux enhancement by spacers in a crossflow reverse osmosis channel, J. Memb. Sci. 284 (2006) 102–109. https://doi.org/10.1016/j.memsci.2006.07.022.

[5] P. Xie, L.C. Murdoch, D.A. Ladner, Hydrodynamics of sinusoidal spacers for improved reverse osmosis performance, J. Memb. Sci. 453 (2014) 92–99. https://doi.org/10.1016/j.memsci.2013.10.068.

[6] A.L. Ahmad, K.K. Lau, Impact of different spacer filaments geometries on 2D unsteady hydrodynamics and concentration polarization in spiral wound membrane channel, J. Memb. Sci.

286 (2006) 77–92. https://doi.org/10.1016/j.memsci.2006.09.018.

[7] K.K. Lau, M.Z. Abu Bakar, A.L. Ahmad, T. Murugesan, Feed spacer mesh angle: 3D modeling, simulation and optimization based on unsteady hydrodynamic in spiral wound membrane channel, J. Memb. Sci. 343 (2009) 16–33. https://doi.org/10.1016/j.memsci.2009.07.001.

[8] A. Shrivastava, S. Kumar, E.L. Cussler, Predicting the effect of membrane spacers on mass transfer, J. Memb. Sci. 323 (2008) 247–256. https://doi.org/10.1016/J.MEMSCI.2008.05.060.

[9] A. Siddiqui, N. Farhat, S.S. Bucs, R.V. Linares, C. Picioreanu, J.C. Kruithof, M.C.M. van Loosdrecht, J. Kidwell, J.S. Vrouwenvelder, Development and characterization of 3D-printed feed spacers for spiral wound membrane systems, Water Res. 91 (2016) 55–67. https://doi.org/10.1016/J.WATRES.2015.12.052.

[10] M. Shakaib, S.M.F. Hasani, M. Mahmood, CFD modeling for flow and mass transfer in spacer-obstructed membrane feed channels, J. Memb. Sci. 326 (2009) 270–284. https://doi.org/10.1016/j.memsci.2008.09.052.

[11] C.P. Koutsou, S.G. Yiantsios, A.J. Karabelas, Direct numerical simulation of flow in spacer-filled channels: Effect of spacer geometrical characteristics, J. Memb. Sci. 291 (2007) 53–69. https://doi.org/10.1016/j.memsci.2006.12.032.

[12] A.L. Ahmad, K.K. Lau, M.Z. Abu Bakar, Impact of different spacer filament geometries on concentration polarization control in narrow membrane channel, J. Memb. Sci. 262 (2005) 138–152. https://doi.org/10.1016/j.memsci.2005.06.056.

[13] J. Schwinge, D.E. Wiley, A.G. Fane, Novel spacer design improves observed flux, J. Memb. Sci. 229 (2004) 53–61. https://doi.org/10.1016/j.memsci.2003.09.015.

[14] V. Geraldes, V. Semiao, M.N. De Pinho, Concentration polarisation and flow structure within nanofiltration spiral-wound modules with ladder-type spacers, in: Comput. Struct., Pergamon, 2004: pp. 1561–1568. https://doi.org/10.1016/j.compstruc.2004.03.052.

[15] V. Geraldes, V. Semiao, M.N. Pinho, Hydrodynamics and concentration polarization in NF/RO spiral-wound modules with ladder-type spacers, Desalination. 157 (2003) 395–402.

https://doi.org/10.1016/S0011-9164(03)00422-3.

[16] V. Geraldes, V. Semião, M.N. De Pinho, Flow management in nanofiltration spiral wound modules with ladder-type spacers, J. Memb. Sci. 203 (2002) 87–102. https://doi.org/10.1016/S0376-7388(01)00753-0.

[17] A.I. Radu, M.S.H. van Steen, J.S. Vrouwenvelder, M.C.M. van Loosdrecht, C. Picioreanu, Spacer geometry and particle deposition in spiral wound membrane feed channels, Water Res. 64 (2014) 160–176. https://doi.org/10.1016/j.watres.2014.06.040.

[18] F. Li, W. Meindersma, A.B. de Haan, T. Reith, Novel spacers for mass transfer enhancement in membrane separations, J. Memb. Sci. 253 (2005) 1–12. https://doi.org/10.1016/J.MEMSCI.2004.12.019.

[19] N. Sreedhar, N. Thomas, O. Al-Ketan, R. Rowshan, H. Hernandez, R.K. Abu Al-Rub, H.A. Arafat, 3D printed feed spacers based on triply periodic minimal surfaces for flux enhancement and biofouling mitigation in RO and UF, Desalination. 425 (2018) 12–21. https://doi.org/10.1016/j.desal.2017.10.010.

[20] N. Yanar, M. Son, E. Yang, Y. Kim, H. Park, S.E. Nam, H. Choi, Investigation of the performance behavior of a forward osmosis membrane system using various feed spacer materials fabricated by 3D printing technique, Chemosphere. 202 (2018) 708–715. https://doi.org/10.1016/j.chemosphere.2018.03.147.

[21] J.Y. Lee, W.S. Tan, J. An, C.K. Chua, C.Y. Tang, A.G. Fane, T.H. Chong, The potential to enhance membrane module design with 3D printing technology, J. Memb. Sci. 499 (2016) 480–490. https://doi.org/10.1016/j.memsci.2015.11.008.

[22] P. Xie, L.C. Murdoch, D.A. Ladner, Mitigating membrane fouling with sinusoidal spacers, Desalin. Water Treat. (2019). Submitted.

[23] Y.Z. Tan, Z. Mao, Y. Zhang, W.S. Tan, T.H. Chong, B. Wu, J.W. Chew, Enhancing fouling mitigation of submerged flat-sheet membranes by vibrating 3D-spacers, Sep. Purif. Technol. 215 (2019) 70–80. https://doi.org/10.1016/j.seppur.2018.12.085.

[24] Z. Han, M. Terashima, B. Liu, H. Yasui, CFD Investigation of the Effect of the Feed Spacer on Hydrodynamics in Spiral Wound Membrane Modules, Math. Comput. Appl. 23 (2018) 80. https://doi.org/10.3390/mca23040080.

[25] S.M. Ali, A. Qamar, S. Kerdi, S. Phuntsho, J.S. Vrouwenvelder, N. Ghaffour, H.K. Shon, Energy efficient 3D printed column type feed spacer for membrane filtration, Water Res. 164 (2019) 114961. https://doi.org/10.1016/j.watres.2019.114961.

[26] R.E. Herrington, Performance of Super Enhanced PEermeate Flow RO Elements with 3D Spacers Printed Directly on the Membrane Surface, (n.d.) 1–22.

[27] J. Schwinge, P.R. Neal, D.E. Wiley, D.F. Fletcher, A.G. Fane, Spiral wound modules and spacers: Review and analysis, J. Memb. Sci. 242 (2004) 129–153. https://doi.org/10.1016/j.memsci.2003.09.031.

[28] G.A. Fimbres-Weihs, D.E. Wiley, Review of 3D CFD modeling of flow and mass transfer in narrow spacer-filled channels in membrane modules, Chem. Eng. Process. Process Intensif. 49 (2010) 759–781. https://doi.org/10.1016/j.cep.2010.01.007.

[29] M.F. Gruber, U. Aslak, C. Hélix-Nielsen, Open-source CFD model for optimization of forward osmosis and reverse osmosis membrane modules, Sep. Purif. Technol. 158 (2016) 183–192. https://doi.org/10.1016/j.seppur.2015.12.017.

[30] J.S. Vrouwenvelder, C. Picioreanu, J.C. Kruithof, M.C.M. van Loosdrecht, Biofouling in spiral wound membrane systems: Three-dimensional CFD model based evaluation of experimental data, J. Memb. Sci. 346 (2010) 71–85. https://doi.org/10.1016/j.memsci.2009.09.025.